Astronomy & Astrophysics manuscript no. fluor_arxiv
March 12, 2014
©ESO 2014

arXiv:1403.2594v1 [astro-ph.GA] 11 Mar 2014

The Chemical Evolution of Fluorine in the Bulge⋆

High-resolution K-band spectra of giants in three fields

H. Jönsson[1], N. Ryde[1], G. M. Harper[2], K. Cunha[3], M. Schultheis[4], K. Eriksson[5], C. Kobayashi[6], V. V. Smith[7], and M. Zoccali[8]

[1] Lund Observatory, Department of Astronomy and Theoretical Physics, Lund University, Box 43, SE-221 00 Lund, Sweden
e-mail: henrikj@astro.lu.se
[2] School of Physics, Trinity College, Dublin 2, Ireland
[3] Observatório Nacional, Rua General José Cristino, 77, 20921-400 São Cristóvão, Rio de Janeiro, RJ, Brazil
[4] Observatoire de la Cote d'Azur, Boulevard de l'Observatoire, B.P. 4229, F 06304 NICE Cedex 4, France
[5] Department of Physics and Astronomy, Uppsala University, Box 516, SE-751 20 Uppsala, Sweden
[6] Centre for Astrophysics Research, University of Hertfordshire, Hatfield AL10 9AB, United Kingdom
[7] National Optical Astronomy Observatory, 950 North Cherry Avenue, Tucson, AZ 85719, USA
[8] Instituto de Astrofisica, Pontifica Universidad Catolica de Chile, Casilla 306, Santiago 22, Chile

Submitted 2014; accepted 2014

ABSTRACT

Context. Possible main formation sites of fluorine in the Universe include AGB stars, the ν-process in Type II supernova, and/or Wolf-Rayet stars. The importance of the Wolf-Rayet stars has theoretically been questioned and they are probably not needed in the modelling of the chemical evolution of fluorine in the solar neighborhood. It has, however, been suggested that Wolf-Rayet stars are indeed needed to explain the chemical evolution of fluorine in the Bulge. The molecular spectral data, needed to determine the fluorine abundance, of the often used HF-molecule has not been presented in a complete and consistent way and has recently been debated in the literature.

Aims. We intend to determine the trend of the fluorine-oxygen abundance ratio as a function of a metallicity indicator in the Bulge to investigate the possible contribution from Wolf-Rayet stars. Additionally, we present here a consistent HF line list for the K- and L-bands including the often used 23358.33 Å line.

Methods. High-resolution near-infrared spectra of eight K giants were recorded using the spectrograph CRIRES mounted at VLT. A standard setting was used covering the HF molecular line at 23358.33 Å. The fluorine abundances were determined using spectral fitting. We have also re-analyzed five previously published Bulge giants observed with the Phoenix spectrograph on Gemini using our new HF molecular data.

Results. We find that the fluorine-oxygen abundance in the Bulge probably cannot be explained with chemical evolution models including only AGB-stars and he ν-process in supernovae Type II, i.e. a significant amount of fluorine production in Wolf-Rayet stars is likely needed to explain the fluorine abundance in the Bulge. Concerning the HF line list, we find that a possible reason for the inconsistencies in the literature, with two different excitation energies being used, is two different definitions of the zero-point energy for the HF molecule and therefore also two accompanying different dissociation energies. Both line lists are correct, as long as the corresponding consistent partition function is used in the spectral synthesis. However, we suspect this has not been the case in several earlier works leading to fluorine-abundances ∼0.3 dex too high. We present a line list for the K- and L-bands and an accompanying partition function.

Key words. Galaxy: bulge – Galaxy: evolution – Stars: abundances – Infrared: stars

1. Introduction

From a nucleosynthetic perspective fluorine is a very interesting element and its cosmic origin is truly intriguing. Its creation and destruction in stellar interiors is very sensitive to the physical conditions (see for example Lucatello et al. 2011), meaning that observations of fluorine abundances can provide strong constraints to stellar models. It will also be possible to observationally constrain the main stellar nuclear production sites of fluorine in the Universe at different epochs and in different stellar populations. To do this, observations of the chemical evolution of fluorine as a function of metallicity for different stellar populations have to be confronted with model predictions.

Theoretical considerations have offered three main production mechanisms which all should work under prevailing conditions during different phases of stellar evolution. Their relative importance at different stages of evolution and in different stellar populations is only starting to be investigated. The different production sites of ^{19}F, the only stable isotope of fluorine, that have been proposed are:

⋆ Based on observations collected at the European Southern Observatory, Chile (ESO programs 71.B-0617(A), 073.B0074(A), and 079.B-0338(A)) and observations obtained at the Gemini Observatory, which is operated by the Association of Universities for Research in Astronomy, Inc., under a cooperative agreement with the NSF on behalf of the Gemini partnership: the National Science Foundation (United States), the National Research Council (Canada), CONICYT (Chile), the Australian Research Council (Australia), CNPq (Brazil), and CONICRT (Argentina), as program GS-2004A-Q-20.

– *ν nucleosynthesis in supernovae Type II (SNe II)*
The core collapse of a massive star, following a SN II explosion, leads to a prodigious neutrino flux. In spite of the small cross sections, the large amount of neutrinos gives rise to a significant spallation of ^{20}Ne to ^{19}F (Woosley & Haxton 1988) in the overlying (neon-rich) shells of the core. Hartmann et al. (1991) estimates the total (mu- and tau-) neutrino energy to $E_\nu = 3{\times}10^{53}$ erg. Kobayashi et al. (2011a) investigate the importance of this total neutrino energy for the ν process reactions for the evolution of fluorine in the solar neighborhood. They conclude that the ν nucleosynthesis should be a major fluorine production mechanism and that its relative contribution is largest for low metallicities.
– *Thermal-pulsing Asymptotic Giant Branch (TP-AGB) stars*
Low-mass ($2 \lesssim M/M_\odot \lesssim 4$) TP-AGB stars have been suggested to produce fluorine in different burning phases during the thermal pulse stage, by nuclear reaction chains starting from ^{14}N (Forestini et al. 1992; Jorissen et al. 1992; Abia et al. 2011; Kobayashi et al. 2011a; Gallino et al. 2010). Fluorine is then transported up to the surface by the 3$^{\rm rd}$ dredge-up. Fluorine production in AGB-stars is expected to be accompanied by the slow-neutron capture nucleosynthesis (the s-process), producing elements like Sr, Y, Zr, Nb, Ba, and La (e.g. Mowlavi et al. 1998; Goriely & Mowlavi 2000; Abia et al. 2009). It has been demonstrated observationally that AGB stars do produce fluorine, see for example Jorissen et al. (1992) and Abia et al. (2011).
– *Wolf-Rayet (W-R) stars*
Meynet & Arnould (1993, 1996, 2000) suggested that W-R stars could contribute significantly to the galactic fluorine budget. ^{19}F is produced in the convective cores of W-R stars, during the core He-burning phase. Due to a large mass loss caused by a metallicity-dependent, radiatively-driven wind, the destruction of ^{19}F by the (α, p) reaction is prevented since the convective core shrinks. The fluorine left behind is eventually exposed at the surface as the heavy mass loss strips the star of the outer layers. This mechanism depends on key parameters, such as initial mass, metallicity, and rotational velocity. Fluorine is produced from ^{14}N, which means that the more ^{14}N is available the more fluorine is expected. A second metallicity-dependent effect is the metallicity-dependent winds. Both circumstances favor the fluorine production at higher metallicities. Palacios et al. (2005) show that when incorporating newer yields and including models of rotating W-R stars, the yields from this mechanism are significantly reduced, implying that W-R stars might not be a major contributor of fluorine. However, they conclude that due to large uncertainties in key nuclear-reaction rates and mass-loss rates, the question of the contribution to galactic ^{19}F from W-R stars is still open.

Using a semi-analytic multizone chemical-evolution model, Renda et al. (2004) show for the first time the impact of the AGB and W-R star contributions to the Galactic chemical evolution of fluorine. They show that ν nucleosynthesis was dominant in the early universe and that AGB stars' significance successively grows. Based on the old yields and non-rotating models, they further show that the contribution of W-R stars is significant for solar and super-solar metallicities, increasing the [F/O] ratio by a factor of two at solar metallicities. Their conclusion is that all three production sites are needed in order to explain the Galactic chemical evolution of fluorine for a range of metallicities.

Kobayashi et al. (2011a) modeled the evolution of fluorine in the solar neighborhood including AGB stars and ν nucleosynthesis with two different neutrino energies ($E_\nu = 3 \times 10^{53}$ erg and $E_\nu = 9 \times 10^{53}$ erg). Note that the contributions from W-R stars are underestimated in these models, because the elements such as C, N, and possibly F that are newly produced and have been lost via stellar winds before supernova explosions are not included. The models show a good agreement with field stars of higher metallicities. At lower metallicities the models cannot reproduce the observations of Li et al. (2013), but still the model that fits best include the ν process with $E_\nu = 3 \times 10^{53}$ erg.

The abundance of fluorine in stars is difficult to measure due to a paucity of suitable spectral lines. Highly ionized F v and F vi lines in the UV have been used by Werner et al. (2005) in extremely hot post-AGB stars and a handful of F i lines between 6800-7800 Å have been used in extreme helium stars and R Coronae Borealis stars (Pandey 2006; Pandey et al. 2008). All other studies we are aware of have been made using HF molecular lines in the K-band and mostly the HF(1 − 0) R9 line at 23358.329 Å.

Relevant for the observations we present in this paper, is the study by Cunha et al. (2008) who present the first study of the chemical evolution of fluorine in the Galactic Bulge, by investigating six red giants in Baade's Window (five of these spectra are re-analyzed in this paper). They find that the fluorine to oxygen abundance ratio in the Bulge follows and extends the solar neighborhood trend. The trend at higher metallicities needs other sources of fluorine in addition to the ν process contribution, which is sufficient at lower metallicities. These are the AGB star and W-R star contributions. By investigating the correlation with abundances of s-process elements, the authors conclude that, for the Bulge, the W-R wind contribution to the fluorine budget should be important and larger than for the Disk. They therefore suggest that W-R stars might have played a vital role in the chemical evolution of the Galactic Bulge.

In this paper, we observationally investigate the chemical evolution of fluorine in the Bulge, by analyzing red giants from three fields. We discuss the relative contributions of the different main nucleosynthetic sites suggested, by comparing with the latest and most updated models for the evolution of fluorine in the Bulge. Our main conclusion is that a significant fluorine production in W-R stars is likely needed to explain the fluorine abundance in the Bulge, meaning that the production in AGB-stars and SNe II is probably not enough.

2. Observations

We have observed eight K giants in the galactic Bulge using the spectrometer CRIRES (Kaeufl et al. 2004; Moorwood 2005; Käufl et al. 2006), mounted on VLT. The K-band observations explored in this paper are, with one exception, of the same stars as the H-band observations analyzed in Ryde et al. (2010), in turn a sub-sample of the full visual sample used in Zoccali et al. (2006), Lecureur et al. (2007), and Barbuy et al. (2013). The basic data of our stars are listed in Table 1 and the Figure 1 shows the location of our three fields (B3, BW and B6) in comparison to the COBE/DIRBE outline of the Galactic Bulge (Weiland et al. 1994) and the micro lensed Bulge dwarfs of Bensby et al. (2013).

The stars were observed with the CRIRES-setting 24/-1/i giving a spectral coverage from approximately 23070 Å to 23510 Å and therefore including the HF-line at 23358.33 Å. The spectral resolution is around R=40000, as determined from narrow telluric lines. The observations were reduced using the CRIRES pipeline and the continua are normalized with the the IRAF task `continuum`. Subsequently, the telluric lines plaguing

Table 1. Basic data for the observed red giants.

Star[a]	OGLE no	RA (J2000) (h:m:s)	Dec (J2000) (d:am:as)	I	$V-I$	H	K
B3-b1	132160C4	18:08:15.840	-25:42:09.83	16.345	2.308	11.525	11.310
B3-b7	282804C7	18:09:16.540	-25:49:26.08	16.355	2.304	11.614	11.351
B3-b8	240083C6	18:08:24.602	-25:48:44.39	16.488	2.427	11.395	11.130
B3-f3	95424C3	18:08:49.628	-25:40:36.93	16.316	2.259	11.676	11.464
BW-f6	392918	18:03:36.890	-30:07:04.30	16.370	2.017	12.043	11.832
B6-b8	108051c7	18:09:55.950	-31:45:46.33	16.290	2.107	11.883	11.653
B6-f1	23017c3	18:10:04.460	-31:41:45.31	15.960	1.941	11.914	11.671
B6-f7	100047c6	18:10:52.300	-31:46:42.18	15.950	1.891	11.904	11.734

Notes.
[a] Using the same naming convention as Lecureur et al. (2007).

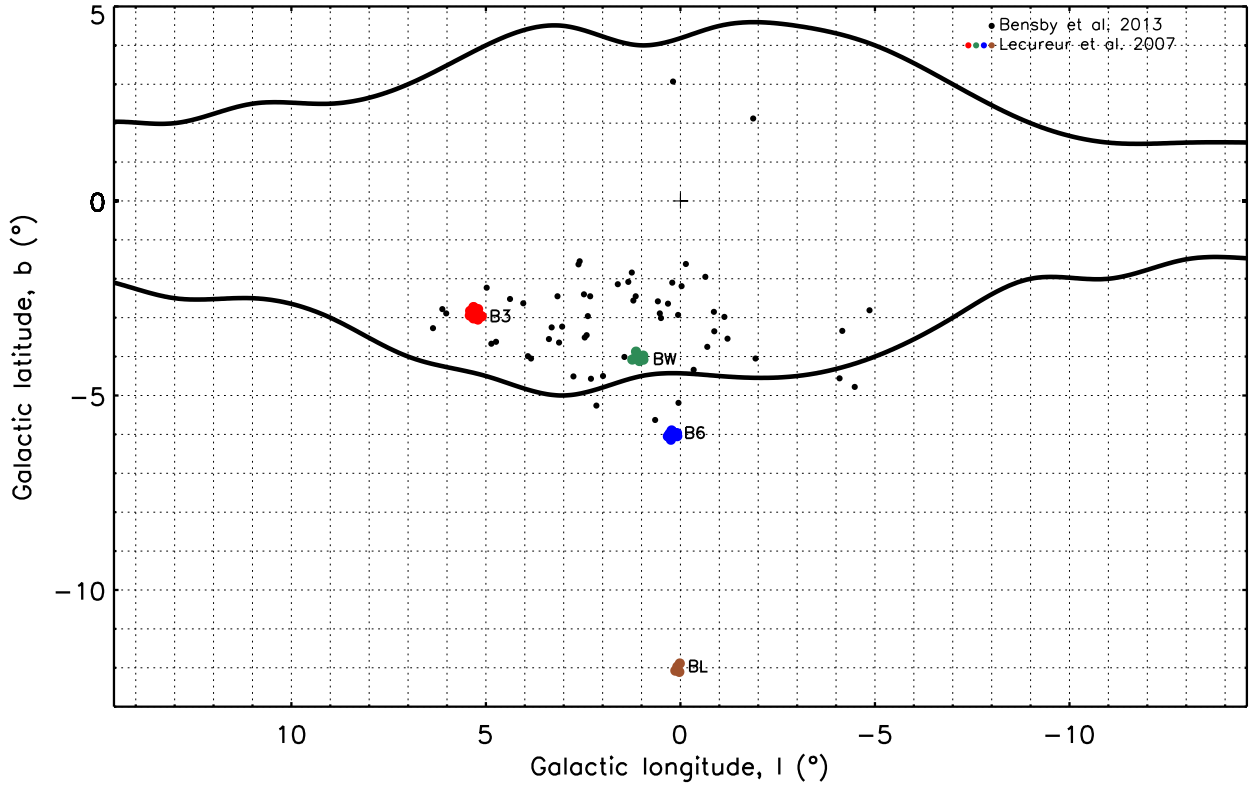

Fig. 1. Location of the four fields (B3, BW, B6, and BL) of Lecureur et al. (2007) in comparison to the COBE/DIRBE outline of the Galactic Bulge (Weiland et al. 1994) and the study of Bensby et al. (2013). Our stellar sample is a subset of the B3-, BW-, and B6-stars. The five re-analyzed stars from Cunha et al. (2008) are in the BW-field.

this part of the IR spectra, were carefully removed by dividing the normalized spectra with that of a telluric standard of high signal-to-noise ratio, which we observed in the same setting and reduced in the same way, using the IRAF task `telluric`.

The stellar parameters were re-determined from the visual observations with the UVES spectrometer described in Lecureur et al. (2007) and the oxygen abundances were re-determined from the H-band data described in (Ryde et al. 2010). The UVES observations were carried out May-Aug 2003-2004 and the CRIRES observations were done May-Aug 2007-2008 and a summary of the observations and the S/N reached, is presented in Table 2. The large optical extinction in the Bulge direction is the cause of the large differences in exposure times between the visual and the infrared observations. The extinction in the K band is a factor of 10 lower that in the V band (Cardelli et al. 1989).

In addition to these eight giants, K-band spectra from three K giants and two M giants in Cunha et al. (2008) (in turn from Cunha & Smith (2006)) have been re-analyzed. These stars are all in Baade's Window and were observed using the Phoenix spectrograph at Gemini-South (Hinkle et al. 1998). For a com-

plete description of these observations, see Cunha et al. (2008) and Cunha & Smith (2006).

Table 2. Summary of the observations with VLT/UVES and VLT/CRIRES.

Star	Total integration time			S/N[a]		
	Visual	*H*	*K*	Visual	*H*	*K*
B3-b1	6h 10m	40m	52m	20	55	44
B3-b7	6h 10m	1h 10m	20m	38	31	37
B3-b8	6h 10m	1h 04m	1h 20m	65	80	79
B3-f3	11h 50m	...	56m	31	...	35
BW-f6	6h 25m	1h 20m	1h 20m	34	46	38
B6-b8	8h 30m	1h 04m	1h 20m	55	35	44
B6-f1	5h 15m	32m	40m	75	33	28
B6-f7	5h 15m	32m	1h 20m	30	42	36

Notes.
[a] S/N per pixel as measured by the IDL-routine `der_snr.pro`, see http://www.stecf.org/software/ASTROsoft/DER_SNR

3. Analysis

The visual, as well as the infrared spectra, were analyzed using the software `Spectroscopy Made Easy`, SME (Valenti & Piskunov 1996). SME simultaneously fits a chosen number of parameters by fitting calculated synthetic spectra to parts of an observed spectrum using χ^2-minimization. The parts, called line masks and continuum masks, mark regions with spectral lines of interest and points which SME should treat as continuum points. The latter are used if a linear rectification in predefined narrow windows of the already continuum-normalized observed spectrum is needed (see Section 2).

SME uses spherical symmetric, [α/Fe]-enhanced, LTE MARCS-models. Within the Gaia-ESO collaboration (Gilmore et al. 2012) it has also been developed to handle NLTE for many iron lines. We have no knowledge of estimated 3D-effects on the fluorine line used in the analysis for our stellar parameters, but Li et al. (2013) have calculated 3D-corrections for more metal-poor stars showing that they are small.

3.1. Stellar parameters

In order to be consistent, we use SME in our analysis, both for our optical and infrared spectra. We have, thus, also redetermined the stellar parameters for our stars based on the method described in Jönsson et al. (in prep.). In short, we determine all the stellar parameters ($T_{\rm eff}$, $\log g$, [Fe/H], and $\xi_{\rm micro}$) simultaneously, with SME using a well-chosen line-list of weak, unblended Fe I, Fe II, and Ca I lines and gravity-sensitive Ca I-wings. All lines except some Fe II-lines have lab-measured oscillator strengths with excellent accuracy (according to the Gaia-ESO line-list categorization of Heiter et al. (in prep.)) and for all iron lines NLTE-corrections have been used. The resulting parameters are listed in Table 3 and are in agreement, within uncertainties, with the ones in Ryde et al. (2010).

In Table 3 we also list the stellar parameters used for the Bulge stars of Cunha et al. (2008) that we re-determine the fluorine abundance for (Cunha & Smith 2006). These stellar parameters are determined from a combination of photometry and IR spectroscopy which might lead to systematic differences to the stellar parameters of the B3-BW-B6 data set. Note also that the two M giants are cooler and have a lower surface gravity than the rest of the stars perhaps leading to systematic differences as well.

Table 3. Determined stellar parameters for the reference star Arcturus and our program stars. Also listed are the stellar parameters of the reanalyzed stars from Cunha et al. (2008).

Star	$T_{\rm eff}$ [K]	$\log g$ (cgs)	[Fe/H][a]	[α/Fe][b]	$\xi_{\rm micro}$ [km s^{-1}]
Arcturus[c]	4262	1.62	−0.63	0.23	1.62
B3-b1	4372	1.11	−1.03	0.39	1.45
B3-b7	4261	1.86	−0.09	0.01	1.57
B3-b8	4282	1.67	−0.75	0.28	1.47
B3-f3	4573	2.55	0.19	0.00	1.76
BW-f6	4117	1.22	−0.54	0.20	1.70
B6-b8	3989	1.30	−0.17	0.05	1.46
B6-f1	4101	1.52	−0.10	0.02	1.65
B6-f7	4221	1.83	−0.41	0.14	1.63
BMB 78[d]	3600	0.8	−0.08	0.01	2.5
BMB 289[d]	3375	0.4	−0.10	0.02	3.0
I-322[d]	4250	1.5	−0.29	0.10	2.0
IV-072[d]	4400	2.4	0.19	0.00	2.2
IV-329[d]	4275	1.3	−0.57	0.21	1.8

Notes.
[a] We use $\log \epsilon(Fe)_{\odot} = 7.50$ (Asplund et al. 2009).
[b] Following the SME MARCS model trends with [α/Fe]=0.4 for [Fe/H]< −1.0, [α/Fe]=0.0 for [Fe/H]> 0.0, and linearly rising in-between.
[c] Spectrum from the atlas by Hinkle et al. (2000).
[d] Stellar parameters from Cunha & Smith (2006).

The uncertainties in our method of determining the stellar parameters from optical spectra and their dependence of S/N will be described in Jönsson et al. (in prep.). In short we have degraded the Arcturus spectrum of Hinkle et al. (2000) to different S/N and determined the stellar parameters for those spectra. The estimated uncertainties for the stars in this paper following this method are $\delta T_{\rm eff} \lesssim 70$ K, $\delta \log g \lesssim 0.2$, δ[Fe/H]$\lesssim 0.1$, and $\delta \xi_{\rm micro} \lesssim 0.1$.

3.2. Line data

All optical line data used in this paper has been collected and/or determined within the Gaia-ESO collaboration (Heiter et al., in prep). The infrared line data except for HF have been extracted from the VALD database (Valenti & Piskunov 1996; Ryabchikova et al. 1997; Kupka et al. 1999, 2000). The line data of the [O I]-line, the three Zr I-lines, and the OH-lines used is listed in Table 4. When it comes to the excitation energies and transition probabilities for HF we calculate them in Section 3.2.1.

3.2.1. HF molecule

The excitation energies and transition probabilities for HF have not been presented previously in a complete and comprehensive manner. The values of Jorissen et al. (1992), who cite private communications with Tipping, are often used. Lucatello et al. (2011), D'Orazi et al. (2013), and Nault & Pilachowski (2013), however, use the excitation energy for the 23358.329 Å-line from Decin (2000), in turn from private communications with Sauval, which differs from the Tipping value by 0.25 eV. As long as the excitation energies and partition functions are con-

Table 4. Atomic and molecular data for the spectral lines used for O and Zr abundance determination.

Element	Wavelength	$\chi_{\rm exc}$	log(gf)	Refs.
Zr I	6127.4400	0.154	-1.060	1
Zr I	6134.5500	0.000	-1.280	1
Zr I	6143.2000	0.071	-1.100	1
[O I]	6300.3038	0.000	-9.715	2,3
OH	15558.021	0.304	-5.309	4
OH	15560.241	0.304	-5.309	4
OH	15565.838	3.663	-4.830	4
OH	15565.961	2.783	-4.700	4
OH	15568.780	0.299	-5.270	4
OH	15572.083	0.300	-5.270	4

References. (1) Biemont et al. (1981); (2) Wiese et al. (1966); (3) Storey & Zeippen (2000); (4) Goldman et al. (1998)

sistent they can both be used for abundance determinations if the corresponding partition function is used. Otherwise there will be an ∼0.3 dex difference in abundance just as Lucatello et al. (2011), D'Orazi et al. (2013), and Nault & Pilachowski (2013) show. Since it is unclear which partition function is used in most works it is difficult to compare the resulting abundance values. In this paper we intend to explicitly present which excitation energies, transition probabilities, and partition function we use so our data can be easily compared with coming studies.

The partition function is defined as:

$$Q(T) = \sum_i g_i \cdot e^{-\chi_i/kT} \tag{1}$$

where $g_{\rm i}$ and $\chi_{\rm i}$ is the statistical weight and the excitation energy of level i. The consistent excitation energies have to be used when calculating the number density of a certain lower level for a transition:

$$\frac{n_{\rm lower}}{n_{\rm total}} = \frac{g_{\rm lower}}{Q(T)} \cdot e^{-\frac{\chi_{\rm lower}}{kT}} \tag{2}$$

The zero point energy of the levels used (which is an issue for molecules but not for atoms), must correspond to the one used to calculate the partition function. Thus, as long as there is not a mis-match, it does not matter which is used since the zero point energies can be factored out in Equation 2.

We use the partition function from MARCS/BSYN and SME (Gustafsson et al. 2008, and references therein), which is an updated version of the one from Sauval & Tatum (1984). This partition function is shown in Equation 3 and in Figure 2.

$$\ln Q(T) = -360.5 + 222.4 \cdot \ln T - 54.6 \cdot (\ln T)^2 + 6.69 \cdot (\ln T)^3 - 0.410 \cdot (\ln T)^4 + 0.00100 \cdot (\ln T)^5 \tag{3}$$

The dissociation energy used is the same as in Sauval & Tatum (1984): $D_0(HF) = 5.869$ eV. We suspect that the 0.25 eV difference between different excitation energies used, comes from the Tipping-list using the dissociation energy of the energy potential, $D_e(HF)$, and not, like Sauval, the true energy required for dissociation, $D_0(HF)$. The former is larger than the latter due to the zero point of the energy of the lowest vibrational level. The difference is indeed 0.25 eV for HF (Zemke et al. 1991a). *We stress once again that it does not matter which energies are used as long as the consistent partition function is used.*

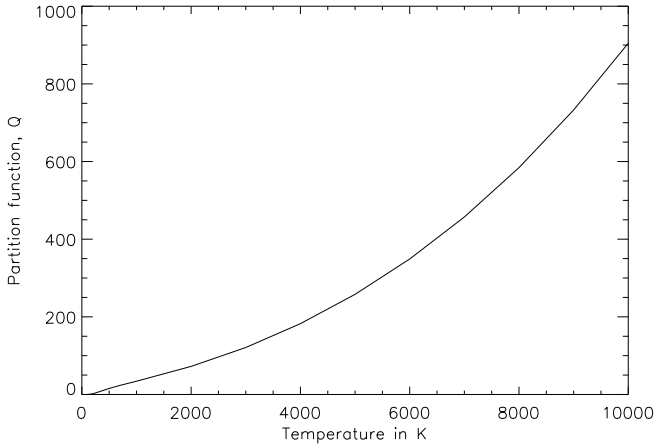

Fig. 2. Partition function of the HF molecule used in the MARCS code and SME for a relevant temperature range.

We have computed the HF line data from available molecular data consistent with the partition function and dissociation energy above. The excitation energies are calculated from the energy-level expression and coefficients of Leblanc et al. (1994). They fitted measured HF-line frequencies to the energy-level expression given by:

$$E(v, J) = T_v + B_v J(J+1) - D_v[J(J+1)]^2 + H_v[J(J+1)]^3 + L_v[J(J+1)]^4, \tag{4}$$

obtaining the rotational constants T_v, B_v, D_v, H_v, and L_v, especially for the vibrational states of interest for us, namely $v = 0$ and $v = 1$. These are provided in Table III of Leblanc et al. (1994). The calculated energy levels are good to $10^{-4}\,{\rm cm}^{-1}$ or better. The excitation energies of the lower energy levels of the ro-vibrational lines of HF are presented in column 6 in Tables 5 and 6.

From this we calculated the transition frequencies (and wavelengths) from the differences of the energy levels of the upper and lower level of the lines. The wavenumbers and wavelengths of the HF lines in the 22700-25000 Å region (R branch, including the band head at 22700 Å) and 25500-39200 Å region (P branch) are given in columns 4 and 5, respectively, in the Tables 5 and 6. The R-branch lines lie in the K band, whereas the P-branch lines originating from higher rotational levels lie in the L band.

We have also computed the HF ro-vibrational Einstein coefficients for spontaneous emission using the transition matix-element expansion coefficients given by Arunan et al. (1992). They used accurate dipole-moment functions based on experimental data to find these coefficients:

$$A_{v'\rightarrow v''}(m) = \frac{64\pi^4}{3\,h}\nu^3 \frac{|m|}{2J'+1} |R_{v'\rightarrow v''}(m)|^2\,, \tag{5}$$

where $m = J'' + 1$ for the R branch, i.e. $J' \leftarrow (J'' - 1)$ and $m = -J''$ for the P branch, i.e. $J' \leftarrow (J'' + 1)$. The upper state is designed with a prime, $'$, and the lower state with a double prime, $''$. The transition matrix elements, $R_{v'\rightarrow v''}(m)$, are given by $R_{v'\rightarrow v''}(m) = a_0 + a_1 m + a_2 m^2 + a_3 m^3$, where the expansion

Table 5. HF line data[a] for the *R branch* ($v' = 1$ and $v'' = 0$).

Line	J'	J''	wavenumber σ	wavelength $\lambda_{\rm air}$	χ_{exc}	χ_{exc}	$A_{v'J',v''J''}$	$\log gf$
R(J'')			[cm^{-1}]	[Å]	[cm^{-1}]	[eV]	[s^{-1}]	
R(0)	1	0	4000.989	24987.001	0.00	0.000	63.42	-4.749
R(1)	2	1	4038.962	24752.082	41.11	0.005	74.07	-4.468
R(2)	3	2	4075.293	24531.418	123.28	0.015	77.02	-4.313
R(3)	4	3	4109.936	24324.642	246.41	0.031	77.29	-4.209
R(4)	5	4	4142.846	24131.413	410.35	0.051	76.26	-4.135
R(5)	6	5	4173.979	23951.417	614.89	0.076	74.47	-4.079
R(6)	7	6	4203.296	23784.365	859.78	0.107	72.19	-4.037
R(7)	8	7	4230.756	23629.991	1144.73	0.142	69.54	-4.004
R(8)	9	8	4256.322	23488.052	1469.37	0.182	66.64	-3.980
R(9)	10	9	4279.960	23358.329	1833.32	0.227	63.53	-3.962
R(10)	11	10	4301.637	23240.623	2236.14	0.277	60.28	-3.950
R(11)	12	11	4321.321	23134.757	2677.32	0.332	56.91	-3.942
R(12)	13	12	4338.986	23040.574	3156.34	0.391	53.46	-3.940
R(13)	14	13	4354.604	22957.938	3672.62	0.455	49.97	-3.941
R(14)	15	14	4368.152	22886.733	4225.54	0.524	46.45	-3.947
R(15)	16	15	4379.608	22826.862	4814.44	0.597	42.94	-3.956
R(16)	17	16	4388.955	22778.249	5438.62	0.674	39.45	-3.969
R(17)	18	17	4396.176	22740.837	6097.33	0.756	36.01	-3.985
R(18)	19	18	4401.256	22714.589	6789.81	0.842	32.64	-4.007
R(19)	20	19	4404.184	22699.488	7515.25	0.932	29.36	-4.031
R(20)	21	20	4404.950	22695.539	8272.80	1.026	26.18	-4.061
R(21)	22	21	4403.548	22702.765	9061.58	1.123	23.13	-4.094
R(22)	23	22	4399.973	22721.213	9880.69	1.225	20.23	-4.133
R(23)	24	23	4394.221	22750.951	10729.19	1.330	17.47	-4.177
R(24)	25	24	4386.294	22792.072	11606.13	1.439	14.89	-4.228
R(25)	26	25	4376.191	22844.690	12510.51	1.551	12.49	-4.286

Notes.
[a] The consistent partition function is given in the text.

coefficients, a_i, are given in a Table VI in Arunan et al. (1992). Finally, the $\log gf$ values are calculated from:

$$\log(gf_{v'J',v''J''}) = \log \frac{(2J'+1)m_e c}{8\pi^2 e^2} \nu^{-2} \cdot A_{v'J',v''J''} \quad (6)$$

see, for example, Larsson (1983). The calculated $\log(gf)$-values are given in column 9 in Tables 5 and 6. Arunan et al. (1992) claim that these transition probabilities are reliable and well-established, and that they are in agreement with *ab initio* calculations of Zemke et al. (1991b), providing confidence in the values.

To get an overview of which lines might be important for abundance determinations, we plot in Figure 3 the relative line strengths in the form of gf $\cdot\, e^{-\chi_{\rm exc}/kT}$ at $T = 4000$ K, a typical temperature of the line forming regions of a red giant. The R9-line used in this and many other works is marked together with some other lines. The equivalent widths of the lines for a typical model atmosphere, show in principle the same relative strengths.

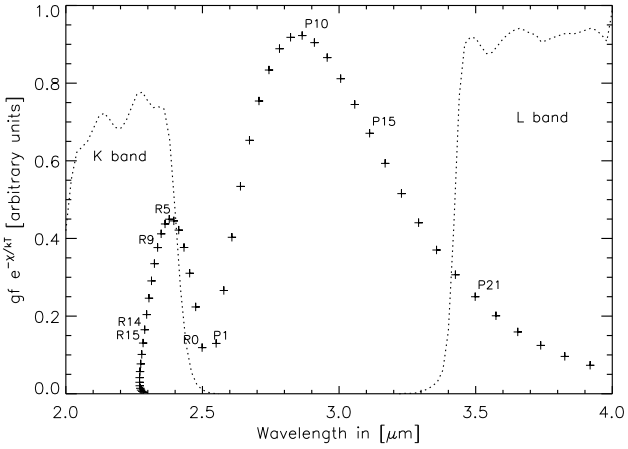

Fig. 3. Relative line strengths of the ro-vibrational HF lines (the R and P branches of the $v'' = 0$ to $v' = 1$ band) given by gf $\cdot\, e^{-\chi_{\rm exc}/kT}$ at $T = 4000$ K. The K and L infrared transmission bands are indicated.

3.3. Stellar abundances

All abundances for the B3-BW-B6 stars were determined using SME and the stellar parameters described in Table 3. The abundances from the visual spectra were determined using the macro-turbulence determined simultaneously as the stellar parameters, but when determining the abundances from the IR-spectra the macro-turbulence was a global free parameter.

The uncertainties in the determined abundances from the uncertainties in the stellar parameters, see Section 3.1, are given in Table 7.

We note that all abundances are most sensitive to the temperature and that they all increase with higher temperature. This will mean that uncertainties, due to the uncertainties in the stellar parameters, in the ratios [F/O] and [Zr/F] used in Figures 6 and 7

Table 6. HF line data[a] for the *P branch* ($v' = 1$ and $v'' = 0$).

Line P(J'')	J'	J''	Wavenumber σ [cm^{-1}]	Wavelength $\lambda_{\rm air}$ [Å]	χ_{exc} [cm^{-1}]	χ_{exc} [eV]	$A_{v'J',v''J''}$ [s^{-1}]	$\log gf$
P(1)	0	1	3920.312	25501.219	41.11	0.005	199.3	-4.711
P(2)	1	2	3877.707	25781.401	123.28	0.015	135.4	-4.393
P(3)	2	3	3833.661	26077.610	246.41	0.031	123.9	-4.199
P(4)	3	4	3788.227	26390.371	410.35	0.051	119.7	-4.058
P(5)	4	5	3741.459	26720.249	614.89	0.076	117.8	-3.945
P(6)	5	6	3693.412	27067.848	859.78	0.107	116.7	-3.850
P(7)	6	7	3644.142	27433.815	1144.73	0.142	116.1	-3.769
P(8)	7	8	3593.705	27818.843	1469.37	0.182	115.5	-3.696
P(9)	8	9	3542.159	28223.674	1833.32	0.227	115.0	-3.632
P(10)	9	10	3489.559	28649.101	2236.14	0.277	114.4	-3.573
P(11)	10	11	3435.964	29095.974	2677.32	0.332	113.7	-3.518
P(12)	11	12	3381.432	29565.205	3156.34	0.391	112.8	-3.468
P(13)	12	13	3326.020	30057.770	3672.62	0.455	111.8	-3.422
P(14)	13	14	3269.785	30574.715	4225.54	0.524	110.6	-3.378
P(15)	14	15	3212.784	31117.163	4814.44	0.597	109.2	-3.337
P(16)	15	16	3155.075	31686.321	5438.62	0.674	107.7	-3.299
P(17)	16	17	3096.715	32283.483	6097.33	0.756	106.0	-3.262
P(18)	17	18	3037.758	32910.043	6789.81	0.842	104.1	-3.228
P(19)	18	19	2978.260	33567.501	7515.25	0.932	102.1	-3.195
P(20)	19	20	2918.275	34257.472	8272.80	1.026	99.94	-3.164
P(21)	20	21	2857.858	34981.701	9061.58	1.123	97.63	-3.134
P(22)	21	22	2797.061	35742.068	9880.69	1.225	95.18	-3.106
P(23)	22	23	2735.935	36540.611	10729.19	1.330	92.61	-3.078
P(24)	23	24	2674.531	37379.535	11606.13	1.439	89.94	-3.053
P(25)	24	25	2612.899	38261.231	12510.51	1.551	87.16	-3.028
P(26)	25	26	2551.086	39188.299	13441.33	1.667	84.30	-3.004

Notes.
[a] The consistent partition function is given in the text.

Table 7. Uncertainties in the determined abundances due to uncertainties in the stellar parameters.

Uncertainty	$\Delta\log\epsilon$(O)	$\Delta\log\epsilon$(F)	$\Delta\log\epsilon$(Zr)
$\delta T_{\rm eff}$ = +70 K	+0.12	+0.15	+0.14
$\delta\log g$ = +0.2	−0.02	+0.01	+0.02
δ[Fe/H]= +0.1	+0.06	−0.03	−0.01
$\delta\xi_{\rm micro}$ = +0.1	−0.01	−0.01	−0.01

will be smaller than the quadratic addition of the two uncertainties. When it comes to the *total* uncertainties in the abundances we also have to include the uncertainties in the continuum fitting around the O-, HF-, and Zr-lines used, but they are in most cases much smaller. Altogether we estimate the total uncertainties in the abundances to approximately 0.15 dex and in the abundance ratios to less than 0.1 dex.

The re-determination of the fluorine abundances for the sample of stars previously analyzed in Cunha et al. (2008) were done using the same LTE MARCS model atmospheres as the B3-BW-B6 stars, but using MOOG (Sneden 1973) instead of SME. Our tests show that, using the same model atmosphere, SME and MOOG give the same result to a very good precision. For a discussion on the uncertainties of the stellar parameters and the abundances of the BMB-I-IV stars, see Cunha & Smith (2006) and Cunha et al. (2008). In particular the most metal-poor star, IV-329, is challenging to analyze due to telluric lines.

4. Results

The part of the spectra containing the lines used in our investigation together with our best fitted synthetic spectra, are presented in Figure 4 and the resulting abundances are presented in Table 8. In Figure 5 we have plotted [F/Fe] and [O/Fe] as functions of [Fe/H] and in Figure 6 we have plotted our abundances together with our chemical evolution models. The fluorine abundances derived here for the stars from Cunha et al. (2008, light-green circles) are systematically lower than those derived previously on account of the different excitation energies and partition functions used (as described in Section 3.2.1), but also because in this study we use newer, alpha-enhanced stellar model atmospheres.

5. Discussion

From the color-coding in Figures 5-7, which designates the three different Bulge fields observed (see Figure 1), we are not able to trace any spatial variation of the fluorine abundance for the different fields. More stars in every field are needed in order to start discussing abundance trends. Therefore, in the following, we will discuss all our abundances as following a general Bulge-trend.

In the right panel of Figure 5 we see the expected decline of oxygen with respect to [Fe/H] due to the large production of iron in SNe type Ia. Our trend follows closely the trend of the micro lensed Bulge stars of Bensby et al. (2013). In the left panel we do *not* see a decline in [F/Fe] for the same range of [Fe/H], and if the upper limit of fluorine abundance in the star B3-b1 is ignored

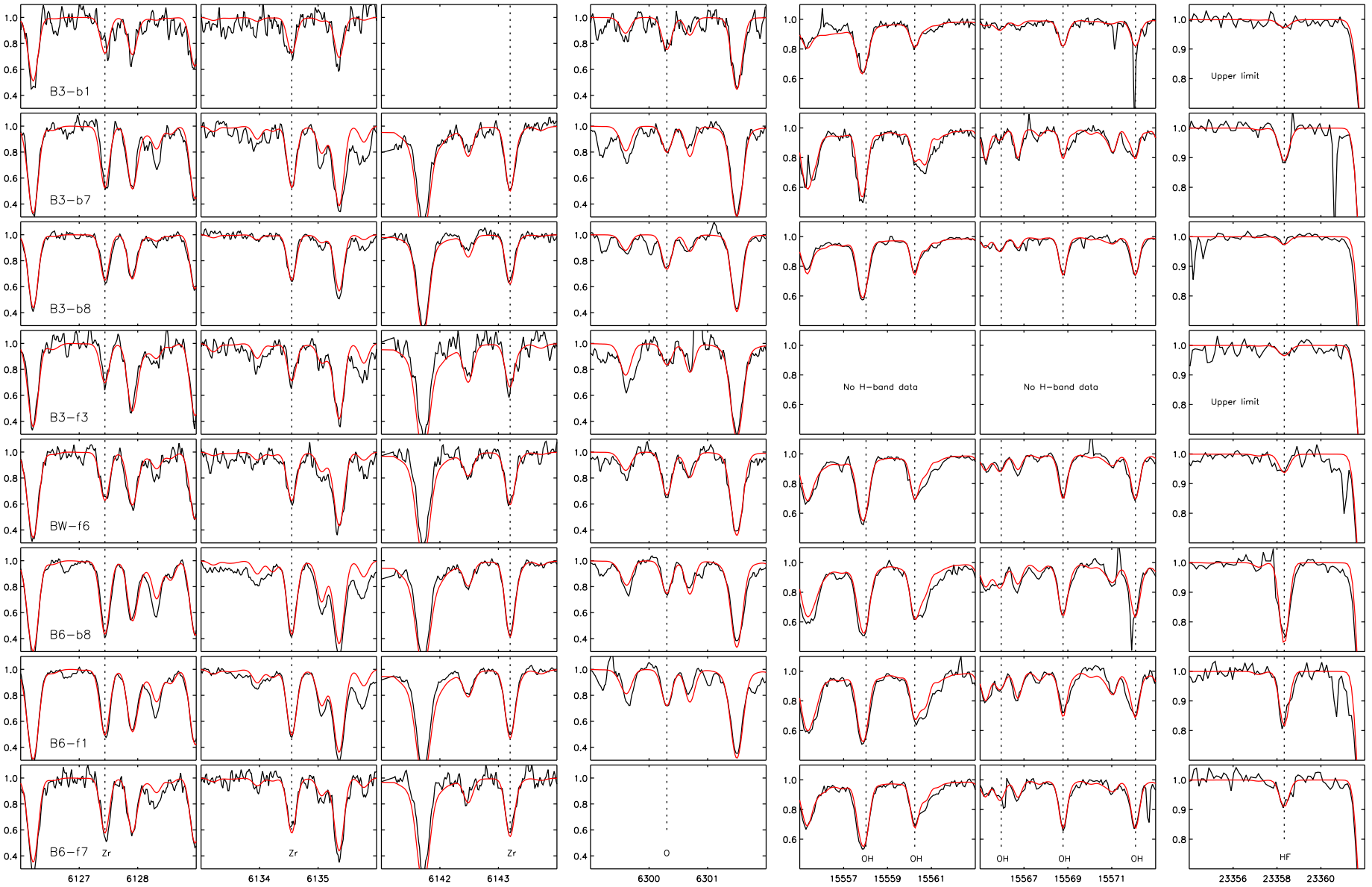

Fig. 4. Observed spectra in black and synthetic spectra in red for the B3-BW-B6 stars. The three Zr-lines, the [O I]-line, the OH-lines, and the HF-line used are marked. The exact wavelengths are listed in Table 4. The OH-lines with obvious cosmic hits have not been included in the fit. Note the different flux scales. An example of the HF-line in the re-analyzed BMB-I-IV can be found in Cunha et al. (2008).

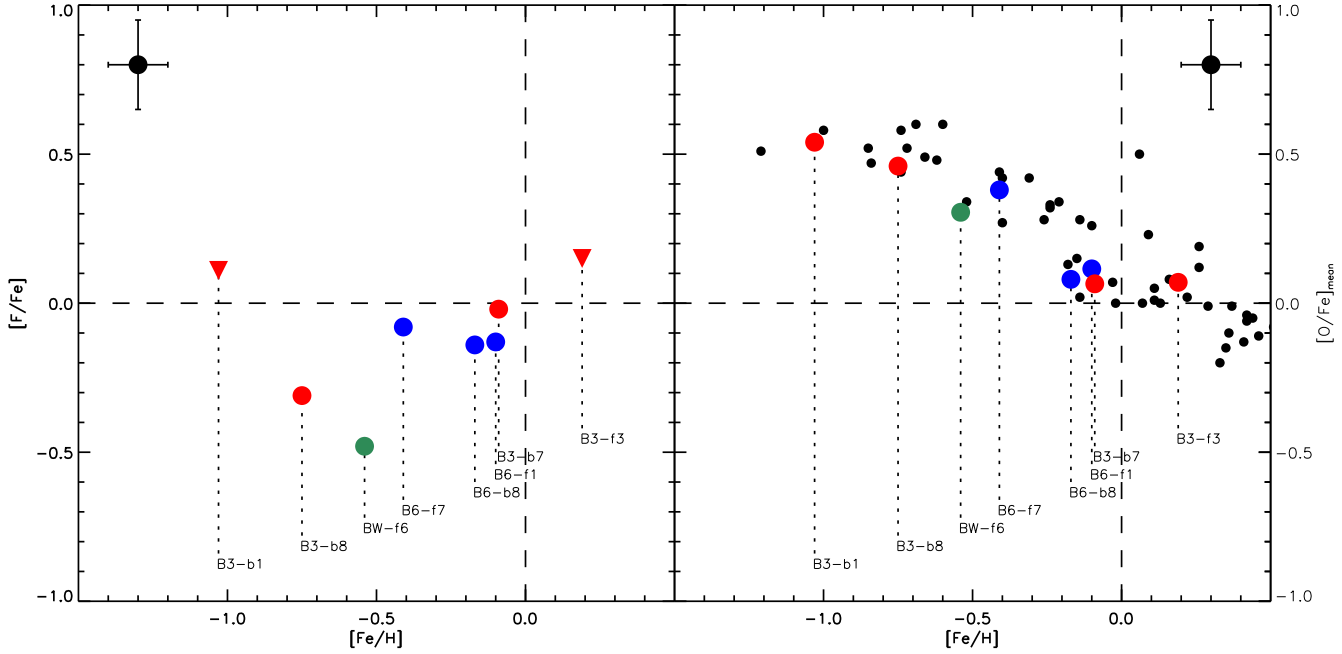

Fig. 5. [F/Fe] and [O/Fe] as functions of [Fe/H] for the B3-BW-B6 stars. The stars are color-coded as the corresponding fields in Figure 1. The black dots are the micro lensed Bulge dwarfs of Bensby et al. (2013) also marked in Figure 1. A conservative estimation of the uncertainties are marked in the upper corners.

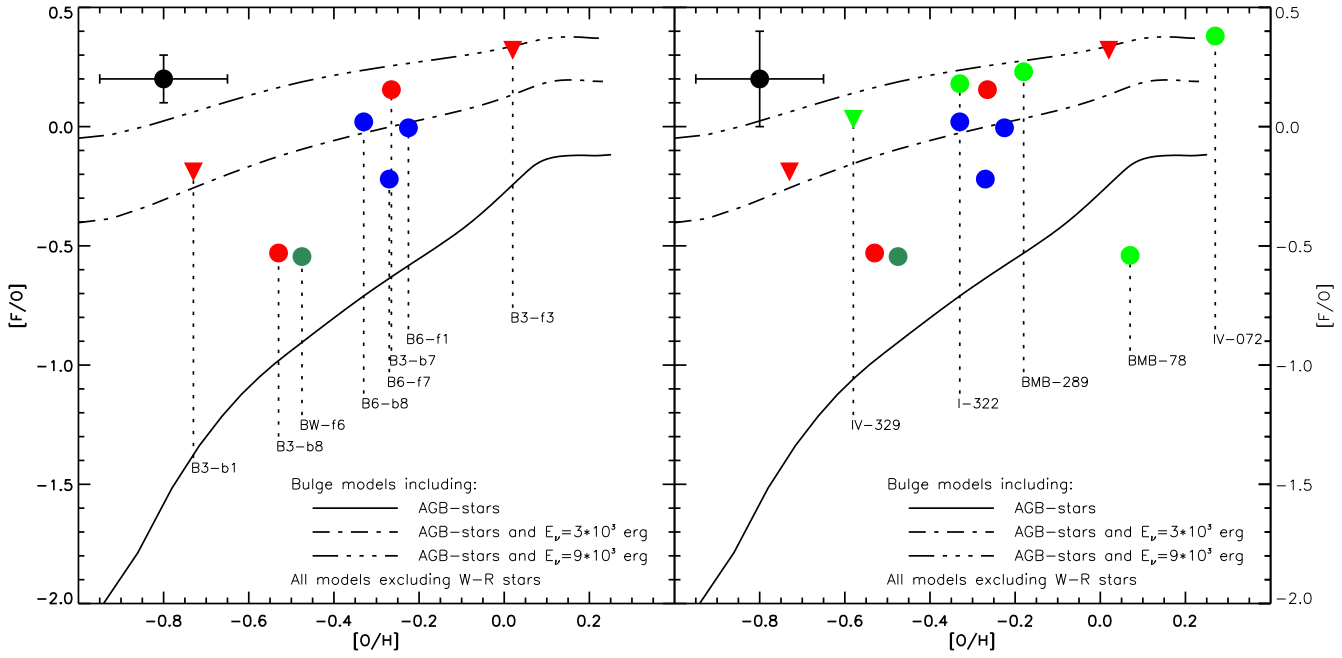

Fig. 6. Our fluorine abundances compared to the predictions of our Bulge models including AGB-stars, excluding *and* including the ν-process with two different energies, and excluding W-R stars. The abundances have been transformed to the scale of the models with $\log \epsilon(F)_\odot = 4.56$ and $\log \epsilon(O)_\odot = 8.93$ (Anders & Grevesse 1989). The stars are color-coded as the corresponding fields in Figure 1 with the BW-stars of Cunha et al. (2008) added in the right panel in a lighter green color. A conservative estimation of the uncertainties are marked in the upper left-hand corners. We note that the star BMB-78, still after the re-analysis, falls below the rest of the trend, see Section 5 for possible explanations.

Table 8. Determined abundances.

Star	$\log\epsilon(O)_{[O\,I]}$	$\log\epsilon(O)_{OH}$	$\log\epsilon(O)_{mean}$	$[O/Fe]_{mean}$[a]	$\log\epsilon(F)$	[F/Fe][a]	$\log\epsilon(Zr)$	[Zr/Fe][a]
Arcturus[b]	8.58	8.47	8.52	0.47	3.75	-0.18	1.8	-0.11
B3-b1	8.11	8.29	8.20	0.54	$\leq$ 3.64	$\leq$ 0.11	2.0	0.53
B3-b7	8.68	8.65	8.66	0.07	4.45	-0.02	2.4	-0.02
B3-b8	8.41	8.39	8.40	0.46	3.50	-0.31	2.1	0.33
B3-f3	8.95	...	8.95	0.07	$\leq$ 4.90	$\leq$ 0.15	2.5	-0.24
BW-f6	8.51	8.40	8.45	0.31	3.54	-0.48	1.8	-0.22
B6-b8	8.54	8.66	8.60	0.08	4.25	-0.14	2.5	0.12
B6-f1	8.73	8.68	8.70	0.12	4.33	-0.13	2.3	-0.13
B6-f7	...	8.66	8.66	0.38	4.07	-0.08	2.2	0.05
BMB-78	...	9.00[c]	9.00[c]	0.39[c]	4.09	-0.39	...	...
BMB-289	...	8.75[c]	8.75[c]	0.16[c]	4.61	0.15	...	...
I-322	...	8.60[c]	8.60[c]	0.20[c]	4.41	0.14	...	...
IV-072	...	9.20[c]	9.20[c]	0.32[c]	5.21	0.46	...	...
IV-329	...	8.35[c]	8.35[c]	0.23[c]	$\leq$ 4.01	$\leq$ 0.02	...	...

Notes.
[a] Using solar abundances of $\log\epsilon(O)_\odot = 8.69$, $\log\epsilon(F)_\odot = 4.56$, $\log\epsilon(Fe)_\odot = 7.50$, and $\log\epsilon(Zr)_\odot = 2.58$ (Asplund et al. 2009).
[b] Spectrum from the atlas by Hinkle et al. (1995).
[c] From Cunha & Smith (2006).

the trend in [F/Fe] increases for the same metallicity range. This would indicate that there must be a production site of fluorine (over-) compensating for the increase in iron around the same time scale as SN type I.

Kobayashi et al. (2011b) model the evolution of fluorine including 'normal' nucleosynthesis in supernovae and synthesis in AGB-stars, excluding the ν-process and yields from W-R-winds for different populations of the Galaxy, including the Bulge. In Kobayashi et al. (2011a) they show models also including the ν-process in SNe II, with two different neutrino energies, but only for the solar neighborhood. The two energies chosen are $E_\nu = 3\times10^{53}$ erg (the energy estimated by Hartmann et al. (1991) and best reproducing the values of Li et al. (2013) in the solar neighborhood) and $E_\nu = 9\times10^{53}$ erg (the theoretically largest possible value). In Figure 6 we present for the first time the combination of the Bulge model as described in Kobayashi et al. (2011b) with the ν-process as modeled in Kobayashi et al. (2011a). If we for the moment ignore the light-green values for the re-analyzed Cunha et al. (2008) stars, we find, just like Li et al. (2013) do for the solar neighborhood, that the fluorine-oxygen abundance trend in the Bulge is *best* described with the model including AGB-stars and $E_\nu = 3\times10^{53}$ erg, but that the models do not to reproduce the trend of the lower-metallicity stars: there seem to be a larger slope in the observed data than in the models, see left panel of Figure 6. This might be due to that the ν-process-contribution in the Bulge is more metallicity-dependent than in the models, or that its contribution in the Bulge is lower and another, more metallicity-dependent source (possibly W-R-stars) is needed.

When including the light-green stars from Cunha et al. (2008), the trend becomes somewhat more scattered, and we treat their fluorine abundance for the star IV-329 as an upper limit. At this star's temperature and metallicity, the HF line is only 4% deep and may be affected significantly by imperfect telluric division. The recent discussion by de Laverny & Recio-Blanco (2013) notes that in low-metallicity stars where the HF R9 line becomes very weak, uncertain telluric-line removal at the 1-2% level (which they maintain is typical) results in large fluorine abundance uncertainties. They suggest caution in interpreting fluorine abundances derived from such a weak HF R9 line. Further, since the figure shows [F/O] as a function of [O/H] the accuracy of the oxygen abundance plays a vital role in defining the trend. As an example of how sever the impact of the oxygen abundance is on the trend of Figure 6 we note that decreasing the oxygen abundance of the peculiar star BMB-78 by 0.3 dex to better follow the B3-BW-B6-stars in Figure 5 will shift it into the B3-BW-B6-trend in Figure 6. The oxygen-abundances of the Cunha et al. (2008) stars will be re-determined using newer, alpha-enhanced model atmospheres to see whether this will influence the [F/O]-trend amongst these stars in Figure 6 (Cunha & Smith, in prep). Presently we cannot rule out that the peculiar fluorine abundance of BMB-78 is a result of inhomogeneous chemical evolution in the Bulge (see Cunha et al. (2008) for further discussion on this). The other Cunha et al. (2008)-stars agree well with the B3-BW-B6 data set in spite of the systematic differences expected from different methods of determining the stellar parameters and the fact that BMB-289 is a M-giant, while the entire B3-BW-B6 data set is made up by K-giants.

To further investigate the possible need of W-R stars to explain the fluorine abundance in the Bulge, we have determined the abundance of the s-element zirconium mainly produced in low-mass AGB-stars (Travaglio et al. 2004) and compared it to the abundance of fluorine, see Figure 7. The negative slope in this plot, showing [Zr/F] as a function of [F/H], suggests that the most fluorine-rich stars have been enhanced in fluorine by a source *not* producing zirconium, i.e. that the contribution from AGB-stars seems small. Thus, the additional sources needed might either be the ν-process, W-R stars, or both. The ν-process does not seem to be metal dependent in our [O/H]-range, while the W-R stars are, meaning that the slope is best explained with W-R stars. However, Zr is not exclusively produced in AGB-stars, but there is some minor r-process and weak s-process production in massive stars as well (Travaglio et al. 2004; Bisterzo et al. 2011). The contribution of these stars to the Bulge Zr-abundance is, as far as we know, not known. To evaluate this further modeling is needed.

Concerning the role of W-R stars for the chemical evolution in the Bulge, it is of interest to compare to the discussion on the oxygen and magnesium trends in the Bulge (for a review, see Rich 2013). Since the metallicity-dependent, radiation-driven winds of W-R stars can be massive and cause

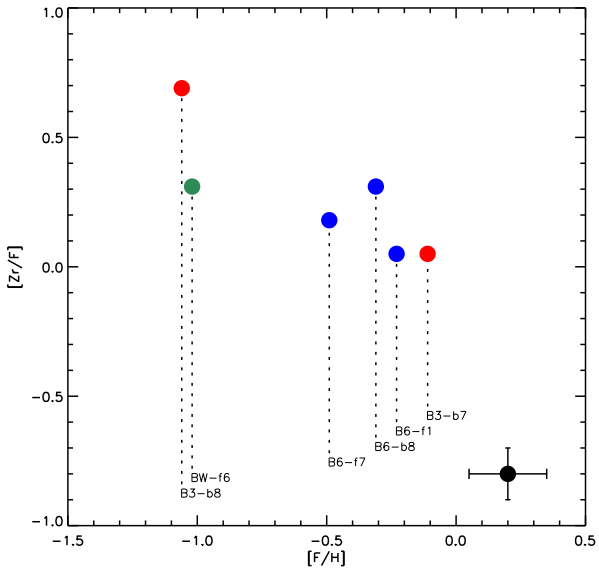

Fig. 7. Abundance ratios of fluorine and zirconium in our sample as a function of the solar normalized fluorine abundance. The negative slope alluded by this plot, suggests that W-R stars might be important for producing fluorine in the Bulge. The stars are color-coded as the corresponding fields in Figure 1 and a conservative estimation of the uncertainties are marked in the lower right-hand corner.

the outer layers of the stars to be pealed off (Maeder 1992), the contribution from these stars could explain the decline of oxygen in the Bulge (Fulbright et al. 2007; McWilliam et al. 2008). At the same time these massive stars could be an important formation site for carbon in the Galaxy (see for example Gustafsson et al. 1999; Mattsson 2010). Fulbright et al. (2007) and McWilliam et al. (2008) discuss the decline in [O/Mg] and [O/Fe] at solar metallicities and Cescutti et al. (2009) the [C/O] versus [O/H] trends in the Bulge, and show that these are best fitted with models including massive star yields altered by metallicity-dependent winds, just as for W-R stars. Note, however, that Alves-Brito et al. (2010) and Ryde et al. (2010) do not find the large increase in the carbon abundance in the Bulge, which would have been expected if the W-R stars had played an important role. Thus, the question of the role of W-R stars in the Bulge is still open. It will, however, be able to be tested with more observations of the sort that already exists. Detailed modeling is needed and improved data may solve this issue (Rich 2013).

Since fluorine is produced from nitrogen in both AGB-stars and W-R stars, while it is produced from neon in the ν-process it would be of interest to investigate the trend of F vs. N in the Bulge, but since our stellar sample is made up by giants it is hard to establish the 'cosmic' nitrogen abundance to the needed accuracy due to newly produced nitrogen being dredged-up into the atmosphere of the star.

6. Conclusion

At low metallicity, our observed fluorine-oxygen abundance trend in the Bulge is lower than predicted in our Bulge model including the ν-process, showing a steeper slope than the model. This might suggest a metal-dependent production source of fluorine. This source cannot be the ν-process in SNe II because it is not metal-dependent over our metallicity range, and it cannot be AGB-stars because these produce s-elements at the same time as fluorine and would probably not give rise to the observed decline in [Zr/F] for increasing [F/H] (as shown in Figure 7). Therefore our data corroborate the findings of Cunha et al. (2008) that W-R stars might be an important source of fluorine in the Bulge. To fully evaluate this we need galactic chemical evolution models that include full sets of yields of AGB stars, W-R stars, and supernova explosions.

We believe that some of the earlier reports of high fluorine abundances might be due to the use of mis-matching molecular data for the HF-molecule, but this has to be investigated. To help with this we have presented a HF line-list with a consistent partition function for lines in the K- and L-bands.

Acknowledgements. This research has been partly supported by the Royal Physiographic Society in Lund, Stiftelsen Walter Gyllenbergs fond and Märta och Erik Holmbergs donation. Also support from the Swedish Research Council, VR, project number 621-2008-4245, is acknowledged. N.R. is a Royal Swedish Academy of Sciences Research Fellow supported by a grant from the Knut and Alice Wallenberg Foundation. N.R. would like to thank the Aspen Center for Physics (and the NSF Grant #1066293) for hospitality during the Bulge/Bar workshop in September 2011, at which part of this work was initiated. M.Z. acknowledges support by Proyecto Fondecyt Regular 1110393, the BASAL Center for Astrophysics and Associated Technologies PFB-06, and by the Chilean Ministry for the Economy, Development, and Tourism's Programa Iniciativa Científica Milenio through grant P07-021-F, awarded to The Milky Way Millennium Nucleus. This publication made use of the SIMBAD database, operated at CDS, Strasbourg, France, NASA's Astrophysics Data System, and the VALD database, operated at Uppsala University, the Institute of Astronomy RAS in Moscow, and the University of Vienna.

References

Abia, C., Cunha, K., Cristallo, S., et al. 2011, The Astrophysical Journal Letters, 737, L8
Abia, C., Recio-Blanco, A., de Laverny, P., et al. 2009, ApJ, 694, 971
Alves-Brito, A., Meléndez, J., Asplund, M., Ramírez, I., & Yong, D. 2010, A&A, 513, 35
Anders, E. & Grevesse, N. 1989, Geochimica et Cosmochimica Acta (ISSN 0016-7037), 53, 197
Arunan, E., Setser, D. W., & Ogilvie, J. F. 1992, The Journal of Chemical Physics, 97, 1734
Asplund, M., Grevesse, N., Sauval, A. J., & Scott, P. 2009, Annual Review of Astronomy and Astrophysics, 47, 481
Barbuy, B., Hill, V., Zoccali, M., et al. 2013, A&A, 559, 5
Bensby, T., Yee, J. C., Feltzing, S., et al. 2013, A&A, 549, 147
Biemont, E., Grevesse, N., Hannaford, P., & Lowe, R. M. 1981, Astrophysical Journal, 248, 867
Bisterzo, S., Gallino, R., Straniero, O., Cristallo, S., & Käppeler, F. 2011, Monthly Notices of the Royal Astronomical Society, 418, 284
Cardelli, J. A., Clayton, G. C., & Mathis, J. S. 1989, Astrophysical Journal, 345, 245
Cescutti, G., Matteucci, F., McWilliam, A., & Chiappini, C. 2009, A&A, 505, 605
Cunha, K. & Smith, V. V. 2006, ApJ, 651, 491
Cunha, K., Smith, V. V., & Gibson, B. K. 2008, ApJ, 679, L17
de Laverny, P. & Recio-Blanco, A. 2013, A&A, 560, 74
Decin, L. 2000, PhD thesis, 16
D'Orazi, V., Lucatello, S., Lugaro, M., et al. 2013, ApJ, 763, 22
Forestini, M., Goriely, S., Jorissen, A., & Arnould, M. 1992, Astronomy and Astrophysics (ISSN 0004-6361), 261, 157
Fulbright, J. P., McWilliam, A., & Rich, R. M. 2007, ApJ, 661, 1152
Gallino, R., Bisterzo, S., Cristallo, S., & Straniero, O. 2010, Memorie della Societa Astronomica Italiana, 81, 998
Gilmore, G., Randich, S., Asplund, M., et al. 2012, The Messenger, 147, 25
Goldman, A., Schoenfeld, W. G., Goorvitch, D., et al. 1998, Journal of Quantitative Spectroscopy and Radiative Transfer, 59, 453
Goriely, S. & Mowlavi, N. 2000, A&A, 362, 599
Gustafsson, B., Edvardsson, B., Eriksson, K., et al. 2008, A&A, 486, 951
Gustafsson, B., Karlsson, T., Olsson, E., Edvardsson, B., & Ryde, N. 1999, A&A, 342, 426

Hartmann, D. H., Haxton, W. C., Hoffman, R. D., & Woosley, S. E. 1991, Nuclear Physics A, 527, 663
Hinkle, K., Wallace, L., & Livingston, W. C. 1995, Infrared Atlas of the Arcturus Spectrum, 0.9-5.3 microns
Hinkle, K., Wallace, L., Valenti, J., & Harmer, D. 2000, Visible and Near Infrared Atlas of the Arcturus Spectrum 3727-9300 A
Hinkle, K. H., Cuberly, R. W., Gaughan, N. A., et al. 1998, Proc. SPIE Vol. 3354, 3354, 810
Jorissen, A., Smith, V. V., & Lambert, D. L. 1992, Astronomy and Astrophysics (ISSN 0004-6361), 261, 164
Kaeufl, H.-U., Ballester, P., Biereichel, P., et al. 2004, in Ground-based Instrumentation for Astronomy. Edited by Alan F. M. Moorwood and Iye Masanori. Proceedings of the SPIE, European Southern Observatory, Germany, 1218–1227
Käufl, H. U., Amico, P., Ballester, P., et al. 2006, The Messenger, 126, 32
Kobayashi, C., Izutani, N., Karakas, A. I., et al. 2011a, The Astrophysical Journal Letters, 739, L57
Kobayashi, C., Karakas, A. I., & Umeda, H. 2011b, Monthly Notices of the Royal Astronomical Society, 414, 3231
Kupka, F., Piskunov, N., Ryabchikova, T. A., Stempels, H. C., & Weiss, W. W. 1999, Astronomy and Astrophysics Supplement, 138, 119
Kupka, F. G., Ryabchikova, T. A., Piskunov, N. E., Stempels, H. C., & Weiss, W. W. 2000, Baltic Astronomy, 9, 590
Larsson, M. 1983, Astronomy and Astrophysics (ISSN 0004-6361), 128, 291
Leblanc, R. B., White, J. B., & Bernath, P. F. 1994, Journal of Molecular Spectroscopy, 164, 574
Lecureur, A., Hill, V., Zoccali, M., et al. 2007, A&A, 465, 799
Li, H. N., Ludwig, H. G., Caffau, E., Christlieb, N., & Zhao, G. 2013, ApJ, 765, 51
Lucatello, S., Masseron, T., Johnson, J. A., Pignatari, M., & Herwig, F. 2011, ApJ, 729, 40
Maeder, A. 1992, Astronomy and Astrophysics (ISSN 0004-6361), 264, 105
Mattsson, L. 2010, A&A, 515, 68
McWilliam, A., Matteucci, F., Ballero, S., et al. 2008, The Astronomical Journal, 136, 367
Meynet, G. & Arnould, M. 1993, Nuclei in the Cosmos; 2: 1992, 503
Meynet, G. & Arnould, M. 1996, Wolf-Rayet stars in the framework of stellar evolution. Liege: Universite de Liege, 33, 89
Meynet, G. & Arnould, M. 2000, A&A, 355, 176
Moorwood, A. 2005, High Resolution Infrared Spectroscopy in Astronomy, 15
Mowlavi, N., Jorissen, A., & Arnould, M. 1998, A&A, 334, 153
Nault, K. A. & Pilachowski, C. A. 2013, The Astronomical Journal, 146, 153
Palacios, A., Arnould, M., & Meynet, G. 2005, A&A, 443, 243
Pandey, G. 2006, ApJ, 648, L143
Pandey, G., Lambert, D. L., & Rao, N. K. 2008, ApJ, 674, 1068
Renda, A., Fenner, Y., Gibson, B. K., et al. 2004, Monthly Notices of the Royal Astronomical Society, 354, 575
Rich, R. M. 2013, Planets, 271
Ryabchikova, T. A., Piskunov, N. E., Kupka, F., & Weiss, W. W. 1997, Baltic Astronomy, 6, 244
Ryde, N., Gustafsson, B., Edvardsson, B., et al. 2010, A&A, 509, 20
Sauval, A. J. & Tatum, J. B. 1984, Astrophysical Journal Supplement Series (ISSN 0067-0049), 56, 193
Sneden, C. 1973, Astrophysical Journal, 184, 839
Storey, P. J. & Zeippen, C. J. 2000, Monthly Notices of the Royal Astronomical Society, 312, 813
Travaglio, C., Gallino, R., Arnone, E., et al. 2004, ApJ, 601, 864
Valenti, J. A. & Piskunov, N. 1996, Astronomy and Astrophysics Supplement, 118, 595
Weiland, J. L., Arendt, R. G., Berriman, G. B., et al. 1994, Astrophysical Journal, 425, L81
Werner, K., Rauch, T., & Kruk, J. W. 2005, A&A, 433, 641
Wiese, W. L., Smith, M. W., & Glennon, B. M. 1966, NSRDS-NBS 4, Washington, D.C.: US Department of Commerce, National Buereau of Standards, 1966
Woosley, S. E. & Haxton, W. C. 1988, Nature (ISSN 0028-0836), 334, 45
Zemke, W. T., Stwalley, W. C., Coxon, J. A., & Hajigeorgiou, P. G. 1991a, Chemical Physics Letters, 177, 412
Zemke, W. T., Stwalley, W. C., Langhoff, S. R., Valderrama, G. L., & Berry, M. J. 1991b, Journal of Chemical Physics (ISSN 0021-9606), 95, 7846
Zoccali, M., Lecureur, A., Barbuy, B., et al. 2006, A&A, 457, L1